Heliyon 9 (2023) e13234

Contents lists available at ScienceDirect

Heliyon

journal homepage: www.cell.com/heliyon

Research article

Pyrolysis of *Canarium schweinfurthii* hard-shell: Thermochemical characterisation and pyrolytic kinetics studies

Kabir Garba [a,*], Isah Yakub Mohammed [a], Yusuf Makarfi Isa [b], Lawan Garba Abubakar [c], Yousif Abdalla Abakr [d], Bassim H. Hameed [e]

[a] *Department of Chemical Engineering, Abubakar Tafawa Balewa University, P. M. B. 0248, Bauchi, Nigeria*
[b] *School of Chemical and Metallurgical Engineering, University of the Witwatersrand, 1 Jan Smuts Avenue, Braamfontein, 2000, Johannesburg, South Africa*
[c] *Department of Agricultural and Bioresource Engineering, Abubakar Tafawa Balewa University, P. M. B. 0248, Bauchi, Nigeria*
[d] *Department of Mechanical, Manufacturing and Material Engineering, The University of Nottingham Malaysia Campus, Jalan Broga, Semenyih, 43500, Selangor Darul Eshan, Malaysia*
[e] *Department of Chemical Engineering, College of Engineering, Qatar University, P. O. Box: 2713, Doha, Qatar*

ARTICLE INFO

Keywords:
Biochar
Bio-oil
Canarium schweinfurthii hard-shell
Kinetics
Pyrolysis
Thermogravimetric analysis

ABSTRACT

Canarium schweinfurthii fruit used in food and cosmetics produces waste nuts with a hard shell (hard-shell) and kernel. The hard-shell contained lignin and holocellulose, besides 51.99 wt% carbon, 6.0 wt% hydrogen, 41.68 wt% oxygen, and 70.97 wt% volatile matter. Therefore, this study commenced thermochemical investigations on the hard-shell through extensive intermediate pyrolysis and kinetic studies. During the active stage of thermogravimetric pyrolysis, the hard-shell lost a maximum of 56.45 wt%, and the activation energies obtained by the Kissinger-Akahira-Sunose, Flynn-Wall-Ozawa, and Starink methods were 223, 221 and 217 kJ/mol, respectively. The Flynn-Wall-Ozawa method depicted the degradation process accurately, where the Coat-Redfern method's contraction and diffusion mechanisms governed the pyrolysis reactions at activation energies of 16.62 kJ/mol and 38.83 kJ/mol, respectively. The pyrolysis process produced 25 wt% biochar and 25 wt% bio-oil under optimum conditions. The calorific values of the bio-oils with 6.81–7.11 wt% hydrogen and 68.01–71.12 wt% carbon was 26.32–27.83 MJ/kg, with phenolics and n-hexadecanoic and oleic acids as major compounds. Biochar, by contrast, has a high carbon content of 75.11–79.32 wt% and calorific values of 25.45–28.61 MJ/kg. These properties assert the biochar and bio-oils among viable bioenergy sources.

1. Introduction

Lignocellulosic biomass, a carbon-neutral renewable resource, can be converted into biofuels and chemicals. In general, it is a more cost-effective, environmentally benign, and sustainable alternative to fossil fuels. To produce biochar and bio-oil, lignocellulosic biomass has recently been converted using thermochemical conversion technologies such as torrefaction, pyrolysis, gasification, hydrothermal carbonisation, and flash carbonisation. The active compounds in biomass undergo intense cross-linking, breakdown, and depolymerisation reactions as a result of these processes [1,2], and the resulting products have a wide range of physicochemical

* Corresponding author.;
E-mail addresses: gkabir@atbu.edu.ng, kbgarba.1214@gmail.com (K. Garba).

https://doi.org/10.1016/j.heliyon.2023.e13234
Received 12 November 2022; Received in revised form 21 January 2023; Accepted 22 January 2023
Available online 25 January 2023

properties [3,4]. Pyrolysis converts biomass by irreversibly changing its physical state and chemical structure when oxygen is absent at sufficient temperatures, frequently exceeding 400 °C [1,4]. Pyrolysis reactors are used to produce biochar, a carbon-rich solid residue and bio-oil composed of phenols and light hydrocarbons, among other chemicals and non-condensable gases. The type and configuration of the reactor influence product distribution and yield as well as the transfer of heat and mass. A multitude of biomass pyrolysis reactors, including using ablative, fluidised-bed, fixed-bed, and auger reactors, are conducted out [1,5]. Owing to their simplicity and low cost for processing a wide range of biomasses, fixed-bed reactors are frequently used to decompose biomass into the three primary products. Bio-oil is a particular focus of research because it is a liquid hydrocarbon that can be used in tandem with fossil fuels to reduce environmental hazards [6]. Furthermore, biochar can be used as a solid fuel in heating systems and boiler furnaces [7,8].

Furthermore, variations in pyrolysis operating conditions have been shown to affect the yield and distribution of pyrolytic products [9,10]. Pyrolysis can be slow, intermediate, or fast depending on the reactor temperature, heating rate, and reaction time. For example, pyrolysis at temperatures above 700 °C with a residence time of about 12 s favoured the production of fuel gas, whereas pyrolysis at a lower temperature, typically around 500 °C, with a shorter hot vapour residence time appeases the production of bio-oil [8]. The slow pyrolysis process, which operates at a lower temperature for a longer residence time, primarily produces biochar through carbonisation [1,11]. Resultantly, the consequences of biomass pyrolysis vary drastically dependent on the species of biomass from which the residue is derived. The pyrolysis route convert lignocellulosic or other biomass to produce bio-oil, which is another biofuel precursor [10,12]. Desert dates [7] and oil palm waste [13] are two examples of thermally decomposed biomass to produce bio-oil. Fast and intermediate pyrolysis, for example, are designed to yield the most bio-oil [7]. When pyrolysis operations are performed in fixed-bed reactors at temperatures of 500–700 °C, the heating rate is risen to between 10 and 30 °C/s, and the maximum yield of bio-oil is produced. However, the amount of vapour produced decreases as the hydrocarbon degrades into compounds with smaller molecular weights at temperatures above 550 °C and for longer periods of time. As a result, the yield of bio-oil decreases. Slow pyrolysis is frequently used to maximise biochar yield at temperatures ranging from 300 to 800 °C with a heating rate of 10 °C/m [14]. Ketones, anhydrosugars, phenolics, acids, furans, benzene derivatives, and other oxygenates are among the important compounds that make up pyrolytic oil, also known as bio-oil. As a result, it can be used as boiler fuel and a source of chemicals with added value [11,15–17]. Furthermore, bio-oil has greater environmental benefits than fossil fuels, such as lower greenhouse gas emissions during combustion. In general, pyrolysis can be used to recover energy from a variety of feedstocks in an economical and sustainable manner. The pyrolysis technique, which is less expensive than landfill disposal, reduces the risk of ground water contamination [18].

The dynamics of lignocellulosic biomass thermal decomposition were investigated using thermogravimetric pyrolysis. Thermogravimetry is an effective technique for expressing the decomposition behaviour of biomass exacerbated by pyrolysis [19–21]. Thermogravimetric evolution curves, among other things, can describe the volatile evolution pattern of decomposing biomass [22,23]. The curves provide crucial data for accurately predicting pyrolysis reactions parameters, such as the activation energy, Arrhenius constant, and devolatilisation index, which explain the kinetics and decomposition behaviour of biomass pyrolysis [24]. The pyrolysis and kinetics of oil palm wastes and *Typha latifolia* were studied using thermogravimetric analysis [25,26]. When compared to other methods, thermogravimetry has the advantage of requiring less data to determine the pyrolysis kinetic parameters of biomass pyrolysis over an assigned temperature range. Because pyrolysis is overwhelmingly reliant on the kinetics and thermodynamics of thermal decomposition reactions [27,28], accurate kinetic and thermodynamic parameters are required for pyrolysis process design. The Coats-Redfern method, a reliable model fitting method, is frequently used to demonstrate biomass degradation kinetics. The method was used to investigate the kinetics of biomass pyrolysis in the absence of a catalyst [29,30]. To predict the kinetics and thermodynamics of biomass pyrolysis, the Coat-Redfern method and model-free, iso-conventional methods such as the Flynn-Wall-Ozawa (FWO), Kissinger-Akahira-Sunose (KAS) and Starink methods are relied on. The methods were used to determine the kinetics and thermodynamic properties of biomass degradation. The Coat-Redfern approach's Gistling-Brounshtein kinetic model and the FWO method, in particular, were successful in accurately predicting the pyrolysis of the *Hyphaene thebaica shell* [31]. The pyrolysis kinetics of poplar wood and waste tire-hazelnut shell pyrolysis were also studied using model-free methods, and the results demonstrated that the complex devolatilisation process was adequately represented by the obtained kinetic parameters [32,33]. Ma et al. [34] predicted the kinetics and thermodynamic properties of hydrochar pyrolysis from co-hydrothermal carbonisation of sawdust and sewage sludge using the FWO and KAS methods. As a result, the experimental kinetics and thermodynamic parameters were found to be in good agreement with the model predictions.

In Plateau State, Nigeria, the *Canarium schweinfurthii fruit (CS)* is widely cultivated for its oil, which is used in both food and cosmetics. The *Canarium schweinfurthii* nut, which consists of a hard shell (hard-shell) enclosing the kernel, is mass-produced and has raised concerns about solid waste disposal. There are substantial gaps in scientific knowledge of the hard-shell kinetics and behaviour during pyrolysis. Despite the fact that several types of lignocellulosic biomass have been thoroughly pyrolysed to this point, little thought has been given to the intermediate pyrolysis of the hard-shell for bioenergy and chemical resources. As a result, this study described the intermediate pyrolysis of the hard-shell in a fixed-bed reactor. The Coats-Redfern method and isoconversional methods were used to determine the kinetic and thermodynamic properties of the pyrolysis reactions. This study presents novel findings concerning the kinetics and degradation parameters of the hard-shell determined through pyrolysis. In the future, the findings will be required to justify the use of the biomass for the production of vast amounts of bioenergy.

2. Materials and methods

2.1. Preparation and characterisation of Canarium schweinfurthii hard-shell and bio-oil

The hard-shell sample, which was generously provided by a trader in Pankshin Township, Plateau State, Nigeria, was ground into

75–500 mesh particles. After drying for 24 h in a 105 °C oven, the samples were sealed in plastic to be used in subsequent pyrolysis testing methods. The compositional parameters of a specified hard-shell sample with 75 mesh particles were ascertained using ultimate and proximate analyses. A CHNO/S analyser (PerkinElmer 400 Series II) was used for the ultimate analysis. By subtracting the amounts of carbon, hydrogen, nitrogen, and sulphur, oxygen was obtained. The hard shell's proximate composition was investigated using a thermogravimetric analyser (PerkinElmer STA 6000) using ASTM D-3172 methods. The results showed the amount of volatile matter (VM), moisture, and ash in the biomass sample, and the difference was used to obtained the fixed carbon (FC). The high heating value (HHV) o the hard-shell was estimated on a bomb calorimeter (IKA C 200). The functional groups on the hard-shell were examined employing Fourier transform infrared (FTIR) spectroscopy with KBr on a Prestige-FITR spectrometer in the 400-4000 cm^{-1} scanning range.

The pertinent compounds in the bio-oils from the hard-shell pyrolysis and their relative compositions were obtained using gas chromatography and mass spectrometry (GC-MS) methods on a PerkinElmer Clarus 600/600T with helium as the carrier gas. The list of identified compounds was derived from the mass spectrum library at the National Institute of Standards and Technology (NIST). The bio-oils physical properties were determined using established techniques described in the literature [7]. The carbon, hydrogen, nitrogen, and sulphur contents of the bio-oils were ascertained using a CHNO/S analyser (PerkinElmer 400 Series II), and the oxygen content was determined using mass balance. Finally, the composition of cellulose, hemicelluloses and lignin in a representative hard-shell sample was determined using published methods [35].

2.2. Thermogravimetric pyrolysis of Canarium schweinfurthii hard-shell

The experiments for the thermogravimetric pyrolysis were implemented on a TGA 50 (Shimadzu) thermogravimetric analyser. The analysis used an exact quantity (5 mg) of the hard-shell sample, which was heated in an aluminium crucible at rates of 5, 10, and 20 °C/min from 30 to 900 °C. To maintain an inert atmosphere for the pyrolysis process, nitrogen gas was passed into the analyser furnace chamber at a rate of 20 mL/min. The hard-shell sample was first heated to 105 °C for 10 min to remove any residual moisture. The heating was kept going until the temperature reached 800 °C. The software program of the analyser was used to determine the data relevant to the decomposition profile and kinetic parameters of the hard-shell pyrolysis at the three heating rates.

2.3. Kinetics study

The decomposition of biomass pyrolysis reaction can be expressed as Eq. (1) based one step global mechanism where:

$$Biomass = Volatiles + Biochar \tag{1}$$

The generic pyrolysis reaction rate as a function of temperature (T) and degree of conversion(α) at constant heating rate (β = dT/dt) is presented as Eq. (2):

$$\frac{d\alpha}{dt} = k(T)f(\alpha) \tag{2}$$

where $\frac{d\alpha}{dt}$ = rate of pyrolysis conversion, T(K) = absolute temperature, $k(T)$ = temperature dependent rate constant, and $f(\alpha)$ = pyrolysis temperature independent conversion function.

The α is the pyrolysis degree of conversion calculated from Eq. (3).

$$\alpha = \frac{w_i - w_t}{w_o - w_f} \tag{3}$$

where w_o is the initial sample weight, w_f is the sample weight of the sample at the end of the reaction, and w_t is the sample weight at any time t. The dependence of K(T) on temperature considering the non-isothermal conditions at constant heating rate is define by the Arrhenius law, Eq. (4).

$$k(T) = A\ exp\left(\frac{-E_\alpha}{RT}\right) \tag{4}$$

where E_α (J/mol) denotes the activation energy, A (1/s) depicts the frequency factor, R (J/mol-K) signifies the universal gas constant, and T (K) is the absolute temperature. A linear temperature profile governs non-isothermal decomposition at a constant heating rate (β), as shown in Eq. (5):

$$T = T_o + \beta t \tag{5}$$

where T_o is the initial temperature and T is the pyrolysis temperature at a time, t. Then, derivate of Eq. (5) gives Eq. (6):

$$\beta = \frac{dT}{dt} \tag{6}$$

The function $f(\alpha)$ associated to the relative conversion α is defined by Eq. (7).

$$f(\alpha) = (1 - \alpha)^n \tag{7}$$

Substituting Eqs. (4) and (5) into Eq. (7), gives:

$$\frac{d\alpha}{dT} = A\ exp\left(\frac{-E_a}{RT}\right)(1-\alpha)^n \tag{8}$$

Therefore, the E_α and A of the pyrolysis reaction can be determined from the Coats-Redfern methods derived from Eq. (8), define as Eq. (9) below:

$$\frac{d\alpha}{dT} = \left(\frac{1}{\beta}\right)A\ exp\left(\frac{-E_\alpha}{RT}\right)(1-\alpha)^n \tag{9}$$

The integral of Eq. (8) is simplified to logarithm expressions as follows:

$$ln\left[\frac{-ln(1-\alpha)}{T^2}\right] = ln\frac{AR}{\beta E_a}\left[1-\frac{2RT}{E_a}\right] - \frac{E_a}{RT} \text{ if n} = 1 \tag{10}$$

or

$$ln\left[\frac{-ln(1-\alpha)^{1-n}}{(1-n)T^2}\right] = ln\frac{AR}{\beta E_a}\left[1-\frac{2RT}{E_a}\right] - \frac{E_a}{RT} \text{ if n} \neq 1 \tag{11}$$

Given that $2RT \rightarrow 0$, Eqs. (10) and (11) becomes Eqs. (12) and (13):

$$ln\left[\frac{-ln(1-\alpha)}{T^2}\right] = ln\frac{AR}{\beta E_a} - \frac{E_a}{RT} \text{ if n} = 1 \tag{12}$$

or

$$ln\left[\frac{-ln(1-\alpha)^{1-n}}{(1-n)T^2}\right] = ln\frac{AR}{\beta E_a} - \frac{E_a}{RT} \text{ if n} \neq 1 \tag{13}$$

Eqs. (10) and (11) modelled the kinetics of the biomass devolatilisation by pyrolysis based on Coats-Redfern ((CR) method. From the linear plots of $ln(f(T,\alpha))$ versus $\frac{1}{T}$ such as $ln\left[\frac{-ln(1-\alpha)}{T^2}\right]$ versus $\frac{1}{T}$ if n = 1 and $ln\left[\frac{-ln(1-\alpha)^{1-n}}{(1-n)T^2}\right]$ versus $\frac{1}{T}$ if n ≠ 1

The slope and intercept can be used to estimate the values of E_α and A. The accuracy of the coefficient of determination (R^2) of the plots establishes the adequacy of the reaction kinetics in describing the devolatilisation reactions. The literature [36,37] contains reaction models based on the CR method for solid material decomposition kinetics.

Biomass degradation by pyrolysis involves a number of reactions that are difficult to describe using a single Coats-Redfern kinetic model. In particular, model-free techniques including Flynn-Wall-Ozawa (FWO), Kissinger-Akahira-Sunose (KAS) and Starink are relied on to predict the pyrolysis kinetics of biomass based on the change in activation energy (E_α) and conversion (α) throughout the pyrolysis process. The KAS model is presented as Eq. (14) [38], obtained by rearranging and taking the natural logarithm of Eq. (13).

$$\ln\left(\frac{\beta}{T^2}\right) = \ln\left(\frac{AE_\alpha}{Rf(\alpha)}\right) - \frac{E}{RT} \tag{14}$$

From the plot of $\ln\left(\frac{\beta}{T^2}\right)$ against $1/T$, E_α is obtained from the slope $\left(-\frac{E_\alpha}{R}\right)$ for each value of α ranging from 0.1 to 0.8. The FWO method, which is based on temperature integration assumption proposed by Doyle, is then represented as Eqs. (15) and (16).

$$f(\alpha) = \frac{A}{\beta}0.00484\ \exp\left(-1.052\frac{E_\alpha}{RT}\right) \tag{15}$$

$$\ln(\beta) = \ln\frac{AE_\alpha}{Rf(\alpha)} - 5.331 - 1.052\frac{E_\alpha}{RT} \tag{16}$$

The Starink method, Eq. (17) [31]is yet another model free method that employs an integral rate equation to describe the biomass pyrolysis.

$$\ln\left(\frac{\beta}{T^{1.92}}\right) = C_s - 1.0033\frac{E_\alpha}{RT} \tag{17}$$

The slopes of the line plots for the KAS, FWO, and Starink methods can be used to estimate the rate of pyrolysis of the hard-shell.

2.4. Pyrolysis of Canarium schweinfurthii hard-shell on a fixed-bed reactor

The hard-shell was intermediately pyrolysed in a fixed-bed reactor with a diameter of 2.54 mm and a height of 35.56 mm. In the reactor, glass wool was used to hold a precise 10 g of the hard-shell sample on a stainless-steel wire mesh. The top of the reactor was then securely tightened with a cap that contained a K-type thermocouple to measure the temperature inside. The reactor was then

surrounded by a vertical furnace that was connected to vapour traps (condensers) that were kept at −2 °C by a circulating chiller. To remove the interior air and maintain an oxygen-free environment for the pyrolysis reactions, 200 mL/min of 99.99% pure nitrogen gas was injected into the reactor for 30 min. The furnace was then heated for an hour at 10° Celsius per minute. The hard-shell inside the reactor was devolatilised into vapour at temperatures ranging from 450 to 600 °C. A series of vapour condensers collected the pyrolysis vapour emitted by the reactor. The condensed vapour's liquid fraction was then collected, while the gas fraction was released into the atmosphere. Following each experiment, the reactor was allowed to cool to room temperature. The gas was estimated using mass balance Eqs. 18–20 with the liquid fraction and the remaining biochar as inputs.

$$\text{Liquid yield (wt\%)} = \frac{\text{Total weight of liquid produced (g)}}{\text{Weight of biomass feedstock utilsed (g)}} \times 100 \tag{18}$$

$$\text{Biochar yield (wt\%)} = \frac{\text{Total weight of biochar produced (g)}}{\text{Weight of biomass feedstock utilsed (g)}} \times 100 \tag{19}$$

$$\text{Gas yield (wt\%)} = 100 - (\%\ \text{liquid yield}) + (\%\ \text{biochar yield}) \tag{20}$$

The weight difference between the liquid trapped before and after each experiment was used to calculate the overall yield of the liquid fraction. The liquid fraction's aqueous and bio-oil phases were separated and weighed separately. The liquid's yields and fractions (bio-oil and aqueous phases) were calculated using Eqs. 21–23 as shown below:

$$Y_L = \left(w_L/w_f\right) \times 100\%\ ;\ Y_a = \left(w_a/w_f\right) \times 100\% \tag{21}$$

$$Y_b = \left(w_b/w_f\right) \times 100\% = Y_a = Y_l - Y_a \tag{22}$$

$$Y_{bc} = \left(w_{bc}/w_f\right) \times 100\%\ ;\ Y_g = 1 - (Y_l - Y_{bc}) \tag{23}$$

3. Results and discussion

3.1. Characterisations of Canarium schweinfurthii hard-shell

Table 1 displays the findings of the proximate and ultimate analyses, as well as the hard-high shell's heating value. The VM of the shell was 70.97 wt%, with low moisture, FC, and ash contents. For biomass pyrolysis conversion, these properties are critical for the shell to decompose and yield enough volatile materials for bio-oil production.

The ultimate analysis showed that the hard-shell was composed of 51.99 wt% carbon, 6.00 wt% hydrogen, and 40.68 wt% oxygen. Notably, the oxygen content is slightly high and comparable to those biomass sources reported in the literature. During by pyrolysis, the oxygen may cause oxygenated compounds to laden the resultant bio-oils with limited viability as a renewable fuel. The shell has a high H/C ratio, a low O/C ratio, and a higher heating value, HHV (18.80 MJ/kg), as revealed in Table 1, which justifies the shell as being suitable for being converted into energy through thermochemical conversion processes.

Additionally, the shell possesses sulphur and nitrogen contents that are comparable to millet chaff and date palm trash [8,39] and may not release much hazardous gases. Nevertheless, when biomass with high amounts of sulphur and nitrogen is utilised in the thermochemical process, there is a risk of considerable environmental pollution from harmful gases emissions. The chemical study shows that the hard-shell contains considerable amounts of hemicellulose, cellulose, and lignin. During the pyrolysis, these components effectively breakdown into volatile matter and biochar.

3.2. Fourier transform infrared analysis of Canarium schweinfurthii hard-shell

The fingerprint and functional groups of the underlying structure on the hard-shell can be deduced from the Fourier transform infrared (FTIR) spectrum shown in Fig. 1. It is possible to distinguish peaks in the spectrum with different intensities that correspond to functional groups. The O–H stretch vibrations are represented by the broad peak surrounding the 3408 cm^{-1} bands. It is believed that

Table 1
Physicochemical characteristics of *Canarium schweinfurthii* hard-shell.

Proximate analysis (dry basis)		Ultimate analysis (dry basis)		Chemical analysis	
Parameter (wt%)	Value	Parameter (wt%)	Value	Component (wt%)	Value
Moisture	3.7	Carbon	51.99	Hemicellulose	31.33
Volatile matter (VM)	70.97	Hydrogen	6.00	Cellulose	28.43
Fixed carbon (FC)	22.37	Nitrogen	0.06	Lignin	39.12
Ash content (AC)	2.96	Sulphur	0.27	Extractives	1.12
HHV (MJ/kg)	18.18	Oxygen	41.68		

phenolic alcohols in the lignin structure and water trapped in the biomass macro-structure are responsible for the broad peak. At the 2926 cm^{-1} band, C–H stretching vibrations were caused by aromatic structural bonds in the lignin structures. Because of the lignin structure's,

syringyl ring, the band elated to the C–O stretching vibration occurred at 1239 cm^{-1}. The C–H bending vibration of cellulose and hemicellulose occurred at a peak in the 592 cm^{-1} band. While the 1739 cm^{-1} and 1627 cm^{-1} bands are attributed to the stretching vibration of the C═O bond in lignin and hemicellulose, respectively. It is understood that the band around 1041 cm^{-1} are associated with stretching vibrations of the C–O, C═C, and C–O–C bonds in cellulose, hemicellulose, and lignin. The spectrum revealed that the majority of the macro-structural units of the hard-shell are composed of compounds with oxygen functional groups related to lignin, cellulose, and hemicellulose structures. The peaks in the spectrum demonstrated how abundant cellulose, hemicellulose, and lignin are in the hard-shell. In comparison to other established biomass, the hard-shell can be pyrolysed for bio-energy generation.

3.3. Thermogravimetric decomposition analysis

The hard-shell degradation caused by pyrolysis was studied using thermogravimetry at temperatures ranging from 32 to 800 °C. The evolution curves of thermogravimetric (TG) and differential thermogravimetric (DTG) decomposition are often used to illustrate the decomposition. The curves were as a result of weight loss caused by volatile compound releases. Fig. 2 depicts the TG and DTG evolution curves for hard-shell degradation at heating rates of 5, 10 and 20 °C/min. The curves revealed three stages of the hard-shell decomposition; the first occurs between 32 and 150 °C with the release of water and light organic compounds held within the biomass cell wall structures, resulting in a weight loss of 7%.

The second stage, which occurred between 180 and 400 °C, was the most active, with a weight loss of 53 wt% due to limited lignin degradation and complete hemicellulose and cellulose degradation. The curves have characteristic steep slopes, indicating a maximum weight loss, due to the significant release of volatile compounds at this stage. As shown in Fig. 3, the extent of conversion is maximal in the second stage, ranging from 71 to 77 wt% between 200 and 435 °C pyrolysis temperatures for the three heating rates. This study validates that the second stage is the most active, yielding the most volatiles.

The third stage occurred at temperatures ranging from 435 to 800 °C. The curves had consistent slopes at this stage, and the slow decomposition of the lignin-rich residual biochar was attributed to the lowest weight loss of 12 wt%. The slow degradation was caused by the massive heat energy required to dissociate the glycosidic bonds in lignin's aromatic structure.

The effect of heating rate on hard-shell decomposition was also investigated during pyrolysis. The TG curves transpose to higher temperatures as the heating rate increased. The DTG curves, however, showed a lateral move, with the peaks moving to higher temperatures as the heating rate increased. Thermal hysteresis caused by heat transfer at different heating rates, and the conductive heat properties of biomass particles, caused the shifts [19]. Similarly, the thermogravimetric pyrolysis of some biomass wastes [20,40] saw their evolution curves shift to higher temperatures as heating increased due to the hysteresis effect.

As depicted in Fig. 2, the decomposition in the second stage increased as the heating rate increase. The enhanced decomposition of the hard-shell particles resulted in the release of more volatile materials. The maximum degradation rate increased by 15.53 wt%, 19.32 wt%, and 21.27 wt% at heating rates of 5, 10, and 20 °C/min respectively. A narrow temperature gradient occurred across the biomass particles at a higher heating rate, typical of 20 °C/min. The heat transfer barrier was eventually overcome and the biomass decomposed rapidly. As a result of the increased release of volatile substances there is a rapid weight loss. A higher heating rate resulted in a higher heat transfer efficiency than a lower heating rate. However, at a low heating rate, especially 5 °C/min, the released volatiles accumulate over a long residence time, which causes them to agglomerate and increase biochar yield.

To further comprehend the hard-shell decomposition via pyrolysis, some characteristic parameters were obtained from the TG and DTG curves and presented in Table 3. Temperatures such as T_i, T_p, $T_{1/2}$, and T_f increased as the heating rate increased from 5 to 20 °C/min. Similarly, the $-R_p$ and $-R_v$ rates significantly increased to higher values. These variations in decomposition parameters are related to heat transfer constraints during the pyrolysis process. As the heat transfer barrier was overcome, the hard-shell decomposition accelerated, resulting in an increased release of volatile matter. The residual weights (Mr) at the end of the pyrolysis decreases as the

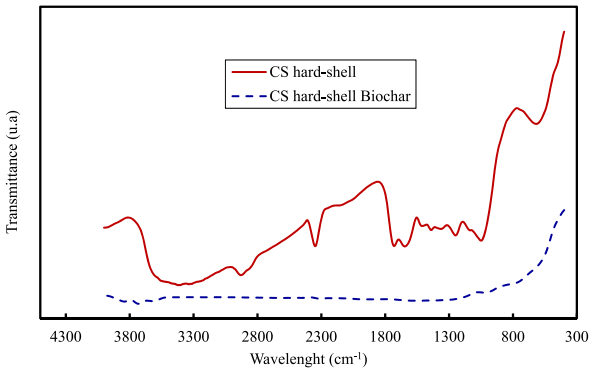

Fig. 1. FTIR spectra of functional groups of ***Canarium schweinfurthii*** hard-shell and its corresponding biochar produced at 550 °C pyrolysis temperature.

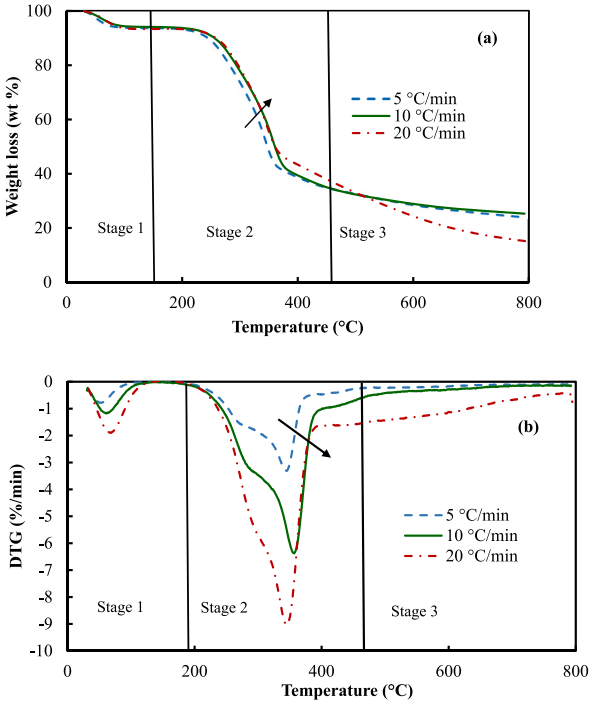

Fig. 2. (a) TG curves and (b) DTG curves for pyrolysis of *Canarium schweinfurthii* hard-shell at different heating rates.

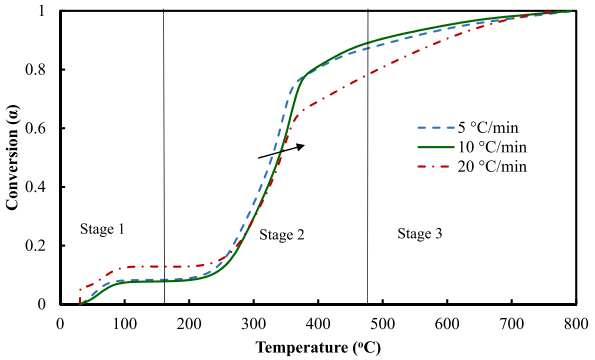

Fig. 3. Extent of conversion for pyrolysis of *Canarium schweinfurthii* hard-shell at different temperatures.

Table 2
Decomposition parameters of *Canarium schweinfurthii* hard-shell at different heating rates.

β (°C/min)	[a]T_i (°C)	[b]T_p (°C)	[c]-R_p (%/min)	[d]-R_v (%/min)	[e]$\Delta T_{1/2}$ (°C)	W_L (wt %)	[f]T_f (°C)	[g]t_f (min)	M_r (wt %)	D ($\%^2°C^{-3}min^{-2}$)	T_{GTotal} (w %)
5	220	346	3.30	1.83	76.00	52.10	385.80	41.40	24.03	1.05E-06	75.97
10	232	358	6.35	2.01	89.00	41.57	395.65	37.10	25.29	1.73E-06	74.71
20	189	345	9.03	3.47	85.00	49.01	390.46	24.40	15.15	5.64E-06	84.86

[a] T_i: Initial decomposition temperature.
[b] T_p: Peak temperature at a stage.
[c] R_p: Maximum weight loss rate of each phase.
[d] R_v: Average weight loss rate.
[e] $\Delta T_{1/2}$: Temperature interval at half value of -R_p.
[f] T_f: Final decomposition temperature and.
[g] T_f:Final decomposition Time.

heating rate increased. At higher temperatures, the short vapour duration limits biochar repolymerization and recondensation reactions [24]. As a result, in the active decomposition stage, the weight loss (W_L) due to volatile release was found to increase with increasing heating rate.

Furthermore, the decomposition index, D, for the pyrolysis degradation of hard-shell was estimated using Eq. (24) [34].

$$D = \frac{\left(-R_p\right) \times \left(-R_v\right) \times M_\infty}{T_v \times T_p \times \Delta T_{1/2}} \tag{24}$$

where $M_\infty = 1 - \left(\frac{M_r}{100}\right)$ and $\Delta T_{1/2} = \left(\frac{T_f - T_i}{2}\right)$

Table 2 displays the index (D) at various heating rates. The index is critical in expressing the pyrolysis performance of the biomass source at each of the three heating rates. The index provides a definitive characteristic of biomass decomposition through the pyrolysis process. The index values revealed the intensity and residence time of the decomposition reaction, beside the extent to which the biomass is passive to thermal decomposition under pyrolysis conditions [41].

3.4. Effect of pyrolysis parameters on products yield

Fig. 4 illustrates how temperature, time, and heating rate affected the product yield from hard-shell pyrolysis. Due to bond cleavage, deoxygenation, and cracking reactions, the shell's holocellulose and lignin structure degrades into three main products: bio-oil, biochar, and gas. As shown in Fig. 4a, the liquid yield varies with temperature between 400 and 600 °C. At a pyrolysis temperature of 550 °C, volatiles are produced and condensed into liquids, yielding a maximum of 44 wt% liquid, containing 25 wt% bio-oil, and 19 wt% aqueous phases.

At higher temperatures, the liquid yield progressively decreased until it remains at 22 wt% at 600 °C. At 450 °C pyrolysis temperature, the hard-shell degraded largely, yielding 30 wt% biochar, 40 wt% liquid (15 wt% bio-oils and 25 wt% aqueous phase), and 30 wt% gas. The biochar was then noticed to decrease from 30 wt% to a minimum of 21 wt% at 600 °C, meanwhile the gas yield improved significantly from 30 wt% to a maximum of 42 wt% at 600 °C. The production of liquid and gas increased at higher temperatures (500–600 °C) due to secondary reactions on the reactive compounds in the pyrolysis vapour, but biochar production significantly reduced due to reductive reactions after attaining a minimum at 600 °C. In addition, the liquid content decreased to its lowest level, whilst gas yield risen to its highest possible level. At high pyrolysis temperatures (over 500 °C), secondary reactions persisted on the high molecular weight compounds of the pyrolysis vapour. Biochar would decompose during the biomass pyrolysis via a reduction reaction, raising the gas fraction. Temperature affects how the hard-shell degrades because heat accelerates the pyrolysis reactions that change the distribution of the end product. This study's findings are strikingly similar to the effects of temperature on the intermediate pyrolysis of desert dates [7] to biochar, gas, and bio-oil. Temperature has a profound influence on product distribution, according to several studies on the pyrolysis of various types of biomass feedstocks. The findings revealed that a high pyrolysis temperature influenced the primary breakdown of the lignocellulosic structure and resulted in secondary reactions that altered the volatiles' production. Their findings substantiated those presented in this study.

Furthermore, the results showed that increasing the pyrolysis time improved the bio-oil yield, as shown in Fig. 4b. Depending on the reaction time, the liquid fraction lasts from 10 to 60 min. A maximum liquid yield of 44 wt% was achieved 30 min into the pyrolysis process. While the biochar yield significantly reduced from 28 to 12 wt% over a 60-min reaction period, the gas generation increased from 33 to 55 wt%. The bio-oil and biochar production fell over the course of 60 min besides the gas surge that revealed the reaction time had a noteworthy impact on the product distributions. This result showed that the secondary reactions had enough time to affect the yield of the residual biochar and composition of the pyrolysis vapour. The highest biochar yield occurred between 10 and 20 min into the pyrolysis process, possibly due to the pyrolysis reactions not having enough time to decompose the biomass feedstock into vapour. As a result, the yield of bio-oil and gas is minimal. Variations in the pyrolysis reaction time had a noticeable effect on the product distribution. As the pyrolysis process progresses to completion, the allied effects of reaction time and heat from the reactor furnace increase. The liquid level rose because there were enough reactions going on to effectively break down the hard-shell. In the lack of sufficient time, however, the hard-shell only partially decomposes, yielding less liquid. Similar results for pyrolysis of various

Table 3
Properties of bio-oils from *Canarium schweinfurthii hard*-shell pyrolysis.

Elemental composition (wt%)	Pyrolysis temperatures (°C)			
	450	500	550	600
Carbon (C)	68.01	68.63	69.17	71.12
Hydrogen (H)	6.81	7.01	6.8	7.11
Nitrogen (N)	1.02	1.17	1.07	1.23
Sulphur (S)	0.12	0.11	0.14	0.25
Oxygen (O)	24.04	23.08	22.82	20.29
O/C	0.35	0.34	0.33	0.29
HHV (MJ/kg)	26.32	26.76	27.6	27.83
pH	3.1	3.2	3.1	3.2
Density (g/mL)	1.21	1.18	1.2	1.23
Viscousity (at 30 °C) (cp)	2.67	2.71	2.81	2.75

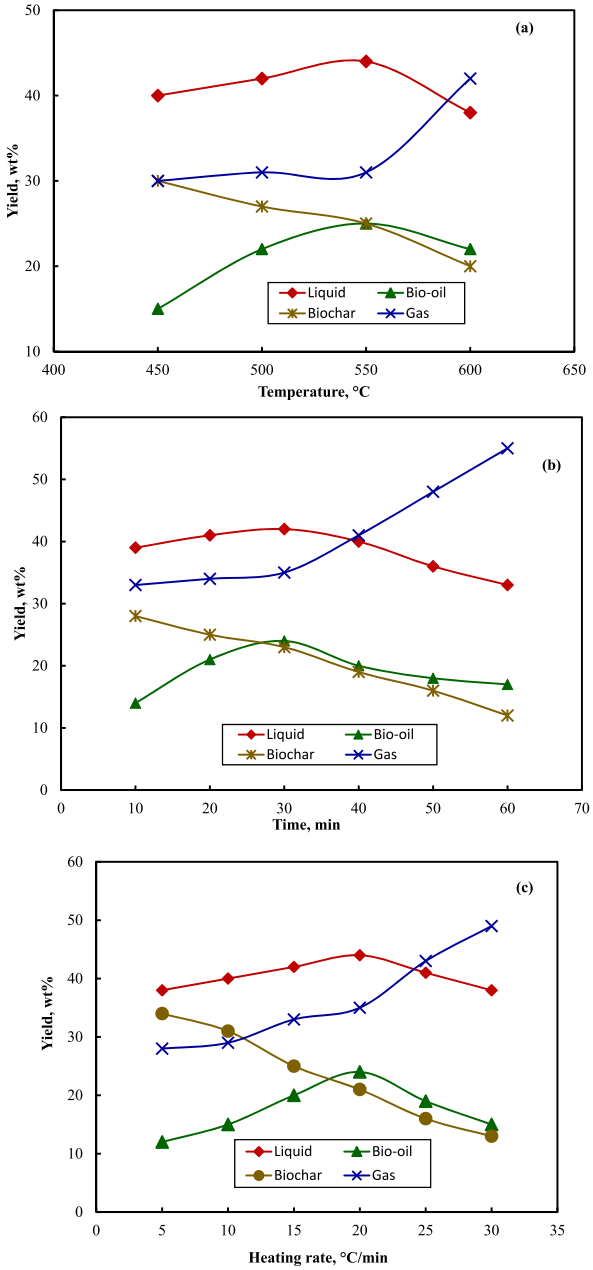

Fig. 4. Effect of (a) temperature, (b) time and (c) heating rate on product yield from pyrolysis of *Canarium schweinfurthii* hard-shell.

biomass sources have been reported in the literature.

The effect of heating rate on product yield was investigated during the pyrolysis was also studied. Accordingly, it was evident that the heating rate had effect on the final products yield and distribution, as demonstrated by Fig. 4c. The best heating rate was 20 °C/min because it produced the most liquid (44 wt%), whilst also 30 °C/min produced the least amount of liquid. Following heating rates higher than the optimum (30 °C/min) restricted liquid and bio-oil yields to a minimum of 38 wt% and 15 wt% respectively. The changes in product distribution were caused by enhanced decomposition of the biomass structure, secondary reactions on the biochar, and rapid heating pyrolysis of vapours to gas, resulting in a corresponding decrease in liquid.

3.5. Bio-oil characterisations and chemicals identification

3.5.1. Bio-oil physicochemical characteristics

Table 3 shows the CHNS, ultimate compositions and HHV of bio-oils derived from the pyrolysis of hard-shell at various

temperatures. The carbon content of the bio-oils ranges from 68.01 to 71.12 wt%, and the oxygen content differs from 24.04 to 20.09 wt%, which is identical to the carbon content of other bio-oils obtained by pyrolysing other biomass sources. Bio-oils contain 35–40% oxygen by weight and are likely to contain a significant amount of oxygenated organic compounds. The high oxygen content of bio-oils marked their low energy density when compared to petroleum-based fuels. The O/C ratio decreases from 0.35–0.29 as the temperature rises to propagated the pyrolysis-related dehydration and oxygenation reactions. As the temperature rises, so did the resultant carbon fraction and calorific values. Nonetheless, because of the significant residual amounts of oxygen, the bio-oils have a lower calorific value than fossil fuels. Because of their high carbon content, VM and HHV, along with low ash, sulphur and nitrogen contents, the bio-oils can be dependable sources of renewable energy. Table 3 also sums up the physical properties of the bio-oils. For the high concentration of heavy oxygenated compounds in bio-oils, the average liquid density at 30 °C was 1.21 g/mL, which was higher than the typical range of 0.75–0.99 g/mL for petroleum-based fuels. The acidity at the low pH of 3.1–3.2 is created by the presence of organic acids and phenolic compounds in the bio-oils. The increase in heating values from 26.32 to 27.83 MJ/kg is largely attributable to the oxygen released during pyrolysis as H_2O, CO, and CO_2 as temperature rises.

3.5.2. *Bio-oil chemical identifications*

Fig. 5 depicts the FTIR spectrum of bio-oil derived from hard-shell pyrolysis. The spectrum contains multiple absorption bands referred to different functional groups of bio-oil compounds. The presence of alcohols and carboxylic acids, as well as moisture trapped in the biomass structure, causes the O–H stretching vibrations associated with the bands between 3231 and 3600 cm^{-1}. The intense peak at 2925 cm^{-1} band and the shoulder at 2975 cm^{-1} band are caused by the symmetric and asymmetric stretching of the C–H bond CH_2 and CH_3 groups, respectively [7,43].

Aliphatic bonding groups were responsible for the C–H bending vibration observed around 1374 cm^{-1} bands and the asymmetric C–H deformation observed between 1430 and 1475 cm^{-1} bands. The bands 1620 to 1680 cm^{-1} correspond to the C═C stretching vibrations of aryl substituted (unsaturated) alkenes. The presence of ketones, carboxylic acids, aldehydes, or esters was revealed by the C═O stretching vibration in the 1700–1770 cm cm^{-1} band range. The presence of alcohol or esters was inferred by the bands at 950 and 1300 cm^{-1} assigned to C–O stretching vibrations. Aromatic stretching vibrations are identified in the bands between 700 and 900 cm^{-1}, implying the presence of aromatic compounds. The functional groups identified by the FTIR analysis indicated that the bio-oil is saturated with oxygenated compounds, which is in accordance with the results of other bio-oils reported in the literature.

The chemical compounds in bio-oils made from *Canarium schweinfurthii* hard-shell were identified using GC-MS at pyrolysis temperatures ranging from 450 to 600 °C. As shown in Fig. 6, the bio-oils constituted a variety of mixtures of different organic compounds. Organic compounds were grouped according to the chemical family to which they belonged. These chemicals characterised the bio-oil's energy density, acidity, high viscousity, corrosiveness, and instability. The acidity is caused by the cellulose and hemicellulose components of the biomass source. According to the literature [42], aromatics are the main products of lignin degradation, which also contribute to acidity and viscousity. The temperature of the pyrolysis affects the composition and yield of the bio-oil. As illustrated in Fig. 6, the relative bio-oil constituents can be categorised into organic acids, esters, phenolics, benzene derivatives, and others. At 600 °C, aromatic production reaches a maximum of 71.81 area%. The aromatic yield evolved considerably when the temperature rose above 550 °C.

As a result, pyrolysis temperatures between 500 and 600 °C were desirable for high aromatic production, notably phenolics and benzene derivatives. It is also clear that changes in pyrolysis temperature have a significant impact on aromatic compound selectivity. Aromatics are critical as industrial intermediates in the production of valuable products such as phenol-formaldehyde resins and liquid fuel additives to reduce reliance on petroleum based alternatives [44]. As shown, only a few aliphatic hydrocarbons, anhydrosugars, PAH, or other compounds, that might be due to peculiar conditions and decomposition reactions during the pyrolysis of the biomass source. Furthermore, the organic acid yield varied from 5 to 10.23% as the pyrolysis temperature increased from 450 to 600 °C.

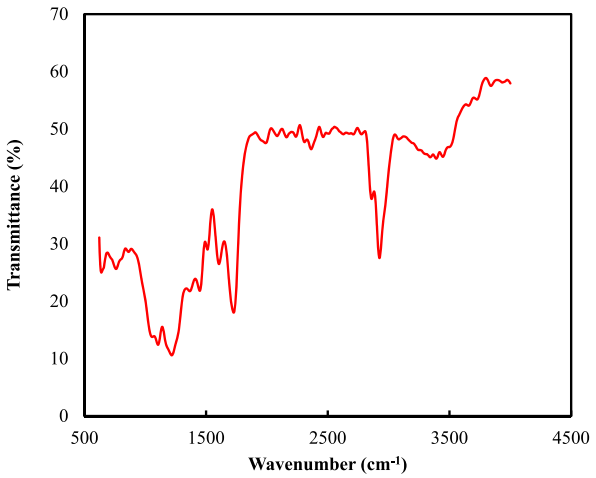

Fig. 5. FTIR spectrum of bio-oil sample from pyrolysis of ***Canarium schweinfurthii*** hard-shell.

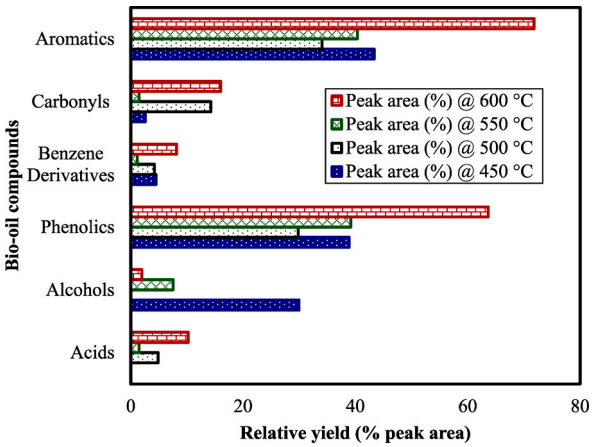

Fig. 6. Relative yield of the categories of tentative compounds in bio-oils from pyrolysis of CS-hard-shell.

Table 4
GC-MS compositions of ***Canarium schweinfurthii*** hard-shell bio-oil (temperature = 600 °C, heating rate = 10 °C/min, and N_2 flow rate = 200 mL/min).

RT (min)	Compounds name	Area %	Empirical formula	Molecular weight (g/mol)
Acids				
48.708	n-Hexadecanoic acid	5.736	$C_{16}H_{32}O_2$	256.424
54.025	Oleic acid	3.531	$C_{18}H_{34}O_2$	282.461
54.696	Octadecanoic acid	0.963	$C_{18}H_{36}O_2$	284.4772
Alcohol				
42.485	3,7-Dimethyl-1,7-octanediol	1.953	$\mathbf{C_{10}H_{22}O_2}$	174.281
Furan derivatives				
61.438	3,3-Dimethyl-2-methylidene-5-propan-2-ylfuran	0.667	$C_{10}H_{16}O$	152.23
Phenols				
13.273	Guaiacol	6.025	$C_7H_8O_2$	124.137
13.973	2-Methylphenol	0.818	$C_7H_8O_2$	108.138
15.399	p-Cresol	3.461	$C_7H_8O_2$	108.138
17.049	4-Methoxy-3-methylphenol	0.188	$C_8H_{10}O_2$	138.164
18.000	Creosol	14.17	$C_8H_{10}O_2$	138.164
19.300	4-Ethylphenol	0.421	$C_8H_{10}O_2$	122.164
21.626	4-Ethylguaiacol	7.764	$C_9H_{12}O_2$	152.190
25.253	Eugenol	6.046	$C_{10}H_{12}O_2$	164.201
23.907	Catechol	5.879	$C_6H_6O_2$	110.1
25.513	2-Methoxy-4-propylphenol	3.981	$C_{10}H_{14}O_2$	166.217
26.003	2-Tert-Butyl-4-(2-phenylpropan-2-yl) phenol	1.415	$C_{19}H_{24}O$	268.393
27.544	*trans*-isoeugenol	0.54	$C_{10}H_{12}O_2$	164.201
27.789	3-Methylcatechol	1.538	$C_7H_8O_2$	124.139
28.609	Vanillin	1.963	$C_8H_8O_3$	152.15
32.896	Methyl vanillate	1.055	$C_9H_{10}O_4$	182.173
33.196	Vanillyl methyl ketone	5.037	$C_{10}H_{12}O_3$	180.201
35.732	1-(2,4-Dihydroxy-3-methylphenyl)-1-propanone	0.478	$C_{10}H_{12}O_3$	180.201
RT (min)	Compounds name	Area %	Empirical formula	Molecular weight (g/mol)
41.685	3-Allyl-2-methoxyphenol	1.976	$C_{10}H_{12}O_2$	164.201
Benzene Derivatives				
22.857	Isoparvifuran	0.109	$C_{16}H_{14}O_3$	254.281
24.903	1,4-Dimethoxy-2,3-dimethylbenzene	3.668	$C_{10}H_{14}O_2$	166.217
34.917	(4-Glycoloylphenoxy) acetic acid	2.258	$C_{10}H_{10}O_5$	210.183
37.488	Methyl 3-(*p*-methoxyphenyl)-2,3-epoxypropionate	0.257	$C_{11}H_{12}O_4$	208.211
Ketones				
10.612	2,3-dimethyl-2-cyclopentenone	0.143	$C_7H_{10}O$	110.154
11.967	2-Methylcyclohexanone	1.52	$C_7H_{12}O$	112.170
Esters				
8.131	2-Methylcyclohexyl acetate	0.262	$C_9H_{16}O_2$	156.222
40.144	3-Dodecanyl acetate	3.211	$C_{14}H_{28}O_2$	228.371
40.999	Methyl 11,13-dihydroxy-5-tetradecynoate	0.645	$C_{15}H_{26}O_4$	270.365

Carboxylate cracking during hemicellulose degradation resulted in significant acid production. The acids are responsible for the undesirable fuel properties of bio-oils, such as instability and corrosiveness. Converting the bio-oils into other value-added materials, on the other hand, can make them appealing as fuel precursors.

3.5.3. GC–MS composition of bio-oil

The chemical composition of the bio-oils was determined using GC-MS analysis of the bio-oil produced at 600 °C pyrolysis temperature. Table 4 provides the potential compounds identified by the NIST library that are tentatively found in the bio-oils. The bio-oil contains a complex mixture of oxygenated molecules, which is essentially consistent with the results of the FTIR analysis. The organic acids, phenolics, ketones, and aldehydes chemical groups are the most abundant in bio-oil. These compounds' molecular weights ranged between 108 and 268 g/mol, while the carbon distribution of these compounds in the bio-oil varied between C_7 and C_{19}. This demonstrates that the bio-oil was viscous due to the presence of high molecular weight oxygenated compounds. Some of the compounds identified here were also present in the bio-oils produced by various pyrolysis processes on biomass. Other notable compounds found in bio-oils from pyrolysis of other biomass [4,11,45] include oleic acid, catechol, guaiacol, creosol, eugenol, vanillyl methyl ketone, and 3-dodecanyl acetate (Table 4). This similarity is thought to be caused by structural components of biomass such as cellulose, hemicellulose, and lignin. The bio-oil contained large faction of phenolics, with a relative composition of approximately 63.65 %Area. The compounds are highly reactive compounds that can help to produce valuable chemicals such as phenol and its derivatives. Given the related %area, the acidic content of the bio-oil was quite significant. The bio-acidity oil was caused by the total relative composition of n-Hexadecanoic acid, oleic acid, and octadecanoic acid, which was roughly 10.23 area%. Therefore, the bio-oil can be corrosive and unstable. There is a need for upgrading prior to long-term storage and use as fuel for heating in boilers and furnaces, however the acids have advantageous industrial applications in the production of emulsifiers for surface coatings [16]. Furthermore, the abundance of acids can make the synthesis of renewable acid chemicals feasible. The high acid content is generally encountered and was also observed in the bio-oil produced from oil palm mesocarp fibre [11]. Upgrading the bio-oil via temperature-programmed stepwise pyrolysis would control acid compositions, while the acids' ketonisation over a catalyst can reduce the acid content of the bio-oil.

3.5.4. Characterisation of Canarium schweinfurthii hard-shell biochar

Table 5 summarises the physicochemical analysis of hard-shell biochar at various temperatures. The values of VM decreased while the values of AC risen as the temperature increased from 450 to 600 °C. At higher temperatures, more VM is released, resulting in thermally stable and non-volatile residual biochar, and the FC becomes markedly larger than in the hard-shell. At the highest pyrolysis temperature, lignin is overwhelmingly degraded into char increasing the value of FC. The ash content in the biomass ranges from 3.03 to 3.48 wt% and can rise due to the presence of inorganic mineral salts.

The concluding analysis was performed to determine the organic element compositions of hard-shell biochar, as shown in Table 5. The analysis revealed that as the pyrolysis temperature increased, the oxygen content of the biochar decreased from 21.11 to 17.26 wt %, indicating that the majority of the oxygenated constituents of the hard-shell were vaporised. While thermal degradation forced to remove oxygen and other volatile substances, biochar produced at various temperatures was found to have a high carbon content. When compared to an equivalent hard-shell, the carbon content of biochar increased from 75.11 to 79.32 wt%. The thermal stability and fuel potential of the biochar can be determined using the ratios $\varphi = \left(\frac{FC}{(VM+FC)}\right)$ and O/C, respectively. With increasing pyrolysis temperature, the φ range from 0.89 to 0.91 and the O/C molar ratio ranged from 0.22 to 0.28 wt%. The biochar had a higher calorific value than the biomass feedstock, ranging from 25.45 to 28.61 MJ/kg, which was comparable to a typical lignite coal found in Nigeria [46]. The biochar was discovered to have a high H/C molar ratio of 0.04–0.05 in the lignite coal zones of the Van Krevelen diagram [47]. This is attributed to changes in the structure of the lignin-rich char caused by scission and cracking reactions, besides an increase in the aromaticity of the biochar, which resulted in the biochar becoming highly carbonised [11]. Because biochar contains less

Table 5
Properties of *Canarium schweinfurthii hard-shell* biochar.

Properties	Pyrolysis temperatures (°C)			
	450	500	550	600
Proximate analysis (dry wt%)				
Moisture	3.89	3.32	2.88	2.77
Volatile matter (VM)	10.42	9.72	8.79	8.64
Fixed carbon (FC)	82.66	83.75	84.92	85.11
Ash content (AC)	3.03	3.21	3.41	3.48
Ultimate analysis (dry wt%)				
Carbon (C)	75.11	76.25	77.36	79.32
Hydrogen (H)	3.58	3.55	3.45	3.33
Nitrogen (N)	0.07	0.08	0.08	0.07
Sulphur (S)	0.13	0.14	0.05	0.02
Oxygen (O)	21.11	19.98	19.06	17.26
H/C	0.05	0.05	0.04	0.04
O/C	0.28	0.26	0.25	0.22
HHV (MJ/kg)	25.45	25.83	27.02	28.61

sulphur and nitrogen than coal, it may emit less hazardous NO_x and SO_x gases during combustion. The biochar can be used as a catalyst and activated carbon, but it can also be a valuable, renewable fuel for boiler and furnace heating.

The FTIR spectrum of the biochar generated at 550 °C is already shown in Fig. 1. When compared to the biomass spectrum, the water molecule's proton vibrations vanished, and the bands between 3200 and 3600 cm^{-1} correspond to the hydroxyl stretching assigned to phenols. Furthermore, the peaks between 1030 and 1300 cm^{-1} bands vanished when compared to the biomass feedstock. Because the majority of bands were missing, this clearly indicates that the biochar had been extensively carbonised. During pyrolysis, the volatile biomass structure was degraded, which increased the C_2 and CH_4 bonds while decreasing the CH and alkyl bonds in the hydrocarbon vapour. Aliphatic bonds eventually evolved into aromatic bonds. The spectrum's multiple peaks representing hard-shell functional groups vanished, demonstrating that aromatics represent the majority of the spectrum.

3.6. Thermo-kinetic studies of Canarium schweinfurthii hard-shell pyrolysis

3.6.1. Estimation of kinetic parameter using model-fitting method

Table 6 shows the kinetic parameters for the most active stage of hard-shell pyrolysis obtained by the Coats-Redfern model-fitting method. The heating rate had a significant effect on the kinetic parameters, as shown in Table 6. With heating rates ranging from 5 to 20 °C/min, the E_α values changed dramatically, with 10 °C/min producing the lowest values. The activation energy was highest at a heating rate of 5 °C/min owing to the accumulation of volatiles over a long period of slow heating. Repolymerization, condensation, and agglomeration of volatile reactive intermediates resulted in the biochar. The highest yield of the residual biochar is conceivable during the pyrolysis process at a heating rate of 5 °C/min. At a heating rate of 20 °C/min, the activation energy decreased marginally, likely to result in secondary decomposition of the volatiles and residual biochar into permanent gases. The biochar yield is lower as compared to at other heating rates. It is important to note that pyrolysis occurs effectively at 10 °C/min heating rate to achieve a significant volatile yield.

3.6.2. Kinetic parameters estimation using model-free methods

The iso-conversional methods, FWO, KAS and Starink methods were adopted to estimate the activation energy dynamics for the pyrolysis of hard-shell at 10 °C/min heating rate. The kinetic parameters A and E_α at different conversion(α) were ascertained using the methods. The activation energy was calculated from the linear plot of ln(β) vs 1/T, ln (βT^2) vs 1/T and ln ($\beta T^{1.92}$) vs 1/T for the FWO, KAS and Starink methods respectively, derived from Eq. (13). The linear plots for the estimation of kinetic parameters are shown in Fig. 7 for the hard-shell pyrolysis. The linear plots of the E_α from FWO (Fig. 7a), KAS (Fig. 7b) and Starink (Fig. 7a) methods exhibited similar trends of parallel lines, attributed by the resembling kinetic behaviour due to identical reaction mechanisms [48].

The changes in A and E_α values with $\alpha = 0.1–0.9$ obtained from the three methods are presented by Fig. 8 and summarised in Table 7. The curves for the change in E_α with $\alpha = 0.1–0.9$ presented in Fig. 8 follow an identical trend for the three methods.

The E_α increases rapidly from $\alpha = 0.05–0.20$ for FWO, $\alpha = 0.05–0.30$ for KAS, and $\alpha = 0.05–0.30$ for Starink, and falls rapidly from 172 to 82 kJ/mol by FWO, from 188 to 157 kJ/mol by KAS until $\alpha = 0.4$ and 188-157 kJ/mol by Starink method. Then, the E_α values increased to a maximum at $\alpha = 0.6$ and fell to a minimum at $\alpha = 0.8$ for all the methods. The low E_α of $= 0.05–0.20$ was attributed to the transition from the moisture removal stage to the devolatilisation of holocellulose in the hard shell. At $\alpha = 0.6$, the E_α reached a maximum of 223 kJ/mol for FWO, 221 kJ/mol for KAS and 213 kJ/mol for Starink, which occurred at 350 °C in the second stage of the pyrolysis. The decomposition in the second stage would consequently need a sizable amount of energy for the pyrolysis reactions to progress, producing a high yield of volatile matter. Thus, the second-stage conversions have the highest E_α values due to the decomposition of the complex structure of the hard-shell.

As outlined in Table 7, E_α varies significantly depending on the conversion reveals that each reaction step owns it activation energy. The apparent activation energy correlation coefficients (R^2) were relatively high, well above 0.97, indicating high accuracy and affirming that the E_α is strongly related to conversions. The E_α values deviated only slightly, and the changing trends were all consistent

Table 6
Kinetics parameters of ***Canarium schweinfurthii*** hard-shell decomposition using Coats-Redfern methods.

Kinetics	5 °C/min			10 °C/min			20 °C/min		
	E_α (kJ/mol)	R^2	A (min^{-1})	E_α (kJ/mol)	R^2	A (min^{-1})	E_α (kJ/mol)	R^2	A (min^{-1})
Chemical reaction mechanisms									
(F1) First Order	24.90	0.9620	2.32E-01	38.15	0.9768	4.45E+00	23.87	0.9362	1.61E-01
(F2) Second Order	36.00	0.9524	4.85E+00	51.80	0.9549	1.48E+02	33.21	0.9272	2.13E+00
(F3) Third Order	49.30	0.9385	1.60E+02	68.25	0.9266	8.99E+03	44.22	0.9153	3.95E+01
Diffusion mechanisms									
(D_1) One-way Transport	41.92	0.9721	3.81E+00	64.72	0.9833	4.36E+02	42.15	0.9582	3.37E+00
(D_2) Two-way Transport	46.99	0.9737	7.41E+00	70.80	0.9847	1.01E+03	46.64	0.9575	5.60E+00
(D_3) Three-way Transport	18.83	0.9597	2.67E-02	30.77	0.9802	4.21E-01	18.63	0.9368	2.35E-02
(D_4) Ginstling-Brounshtein Eq	48.99	0.9739	2.79E+00	73.22	0.9847	4.11E+02	48.37	0.9570	1.96E+00
Nucleation									
(A_4) Avarami-Erofe'ev	0.93	0.3946	6.49E-05	2.38	0.7753	3.17E-04	1.20	0.4283	7.98E-05
Contracting mechanisms									
(C_1) Area contracting	32.42	0.9614	5.71E-01	32.49	0.9805	5.00E-01	26.14	0.9646	9.32E-02
(C_2) Volume contracting	33.68	0.9796	4.84E-02	34.29	0.9800	5.38E-01	24.57	0.9662	5.73E-02

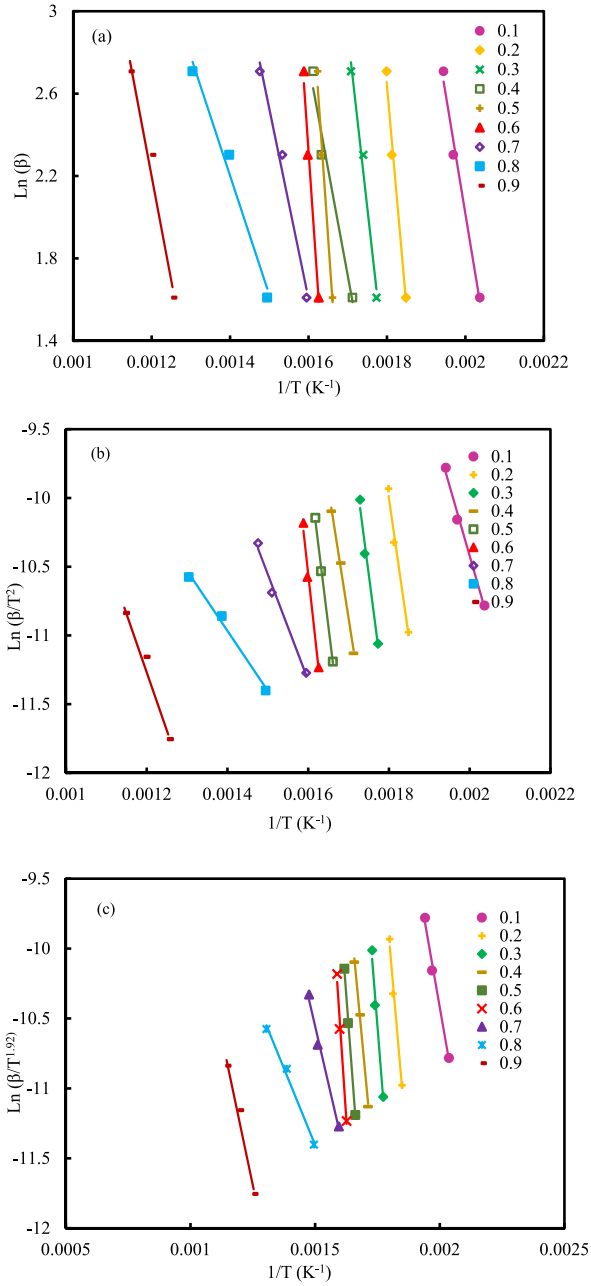

Fig. 7. (a) FWO, (b) KAS and (c) Starink linear plots.

across the three methods, as shown in Fig. 8 and Table 7. The variation in E_α with conversion indicated that the hard-shell pyrolysis was a multiple set of reactions. While low E_α reactions require little energy and progress quickly, those with higher activation energy will eventually slow down.

3.6.3. Thermodynamics properties of Canarium schweinfurthii hard-shell pyrolysis

Table 7 and Fig. 9 demonstrate the results of the thermodynamic parameters enthalpy (ΔH), Gibbs free energy (ΔG), and entropy (ΔS) estimated using FWO, KAS, and Starink techniques. The ΔH is the energy lost or gained by the biomass during its pyrolysis conversion to the major products, illustrated in Fig. 9a. The ΔH ranges from −13.81 to 169.41 kJ/mol according to FWO, −23.62–170.58 kJ/mol as per KAS, and −26.11 to 167.67 kJ/mol according Starink. Endothermic reactions were fully liable for the hard-shell degradation, as indicated by the positive ΔH values (Table 7). A small energy gap of 5 kJ/mol existed between the ΔH and E_α, denoting the prospect of forming an activated complex responsible for viable reactions that may occur during pyrolysis [19,26]. An energy gap lesser than 5 kJ/mol increases the likelihood that products can indeed be formed with a lower energy barrier [49], making

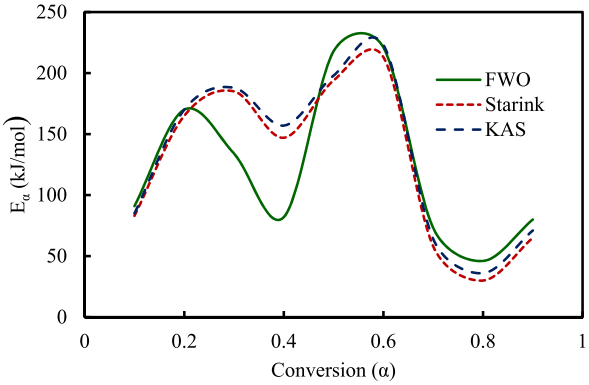

Fig. 8. Variation of apparent activation energy with conversion for pyrolysis of *Canarium schweinfurthii* hard-shell from FWO, KAS and Starink methods.

Table 7
Kinetics and thermodynamics parameters with conversion calculated from the FWO, KAS and Starink methods (conditions: temperature = 550 °C, heating rate = 10 °C/min, and N_2 flow rate = 200 mL/min).

T	A	E_α	R^2	A	ΔH	ΔG	ΔS
(K)		(kJ/mol)		(s^{-1})	(kJ/mol)	(kJ/mol)	(kJ/mol)
FWO							
507.8	0.1	91	0.988	4.35E-04	48.97	159387	−313.78
551.8	0.2	170	0.987	6.99E-04	124.51	171474	−310.53
574.8	0.3	134	0.983	5.01E-04	86.15	180356	−313.62
612.3	0.4	82	0.971	2.66E-04	30.7	195610	−319.42
612.8	0.5	218	0.975	7.29E-04	167.06	190776	−311.05
625.8	0.6	221	0.984	7.10E-04	169.41	195070	−311.44
652.2	0.7	73	0.983	2.09E-04	18.78	209988	−321.94
715.3	0.8	46	0.981	1.08E-04	−13.81	234743	−328.19
833.5	0.9	80	0.975	1.40E-04	10.59	272836	−327.33
Average		123.89			71.3733	201138	−317.48
Starink							
507.8	0.1	83	0.983	4.01E-04	41.27	159551	−315.13
551.8	0.2	165	0.988	6.87E-04	119.26	170330	−311.24
574.8	0.3	185	0.991	7.03E-04	132.26	176212	−311.52
594.8	0.4	147	0.989	5.11E-04	108.78	193478	−315.15
612.8	0.5	194	0.986	6.30E-04	138.53	177500	−311.93
625.8	0.6	218	0.991	7.05E-04	167.67	191000	−312.34
662.2	0.7	58	0.985	1.72E-04	5.02	210123	−321.41
721.3	0.8	30	0.987	8.31E-05	−26.11	232113	−329.81
836.5	0.9	65	0.989	1.92E-04	3.42	267325	−330.65
Average		127.22			76.6778	197515	−317.69
KAS							
507.8	0.1	85	0.992	4.05E-04	42.88	159679	−314.37
551.8	0.2	170	0.985	6.97E-04	124.25	171480	−310.54
574.8	0.3	188	0.981	7.11E-04	139.97	178742	−310.72
594.8	0.4	157	0.994	5.49E-04	107.09	186368	−313.15
612.8	0.5	198	0.997	6.60E-04	147.11	191265	−311.88
625.8	0.6	223	0.983	7.14E-04	170.58	195043	−311.4
662.2	0.7	64	0.989	1.78E-04	9.07	214173	−323.41
721.3	0.8	36	0.99	8.46E-05	−23.62	238229	−330.31
836.5	0.9	71	0.981	1.23E-04	1.09	274749	−328.45
Average		132.44			79.8244	201081	−317.14

pyrolysis products more available.

The ΔG characterises the energy readily accessible from the hard-shell pyrolysis. Presented in Fig. 9b and Table 5, the change patterns and values of the ΔG at different heat treatment rates calculated by FWO, KAS and Starink were found to be consistent. These values indicate that the pyrolysis process generated a substantially stable amount of energy. In comparison, the average ΔG values of rice bran (167.17 kJ/mol), rice straw (164.59 kJ/mol) and waste red pepper (139.4 kJ/mol) [26] were higher. As a result, the hard-shell degraded faster than the other three biowastes, providing more energy. The results of ΔS from the FWO, KAS and Starink methods are shown in Fig. 6c, which revealed the disorder of matter and energy during the pyrolysis process.

The average ΔS values from isoconversional methods were found to be around −317.0 kJ/mol. Because there are multiple reactions

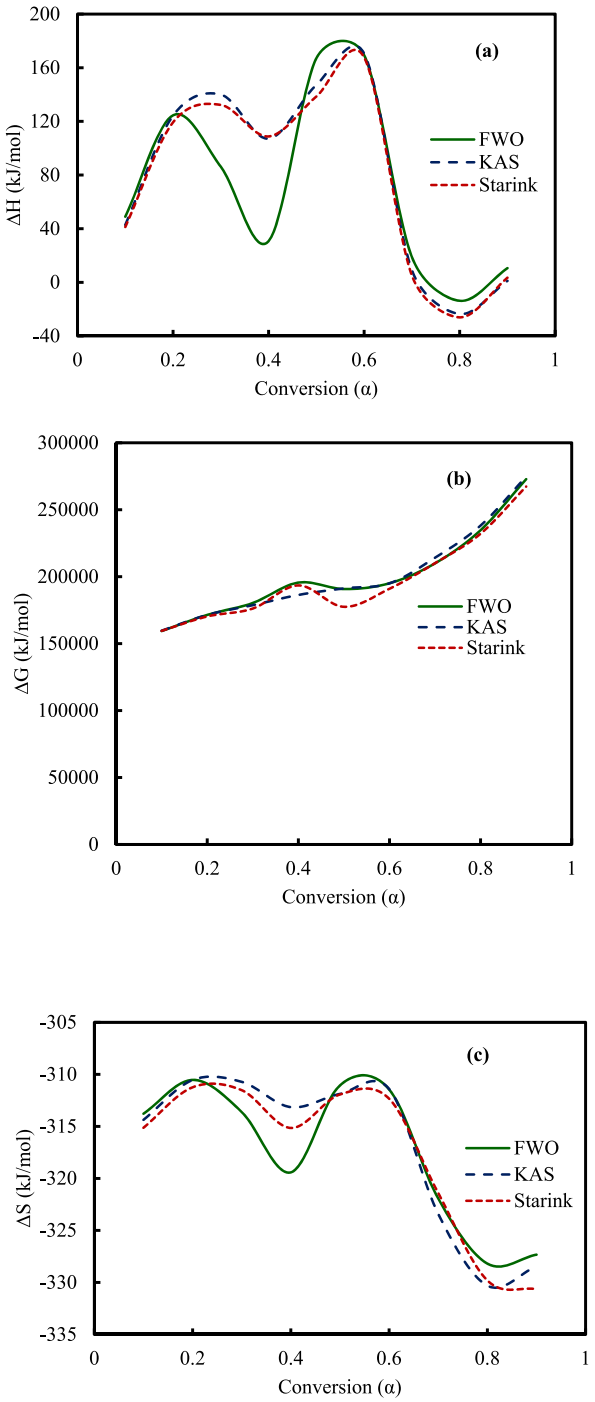

Fig. 9. Variation of (a) ΔH, (b) ΔG and (c) ΔS with extent of conversion for pyrolysis of *Canarium schweinfurthii* hard-shell.

during pyrolysis degradation, negative ΔS values are conceivable. The negative values represent that the products' bond dissociation was less disordered than the original reactants. The low ΔS values indicate that the biomass source approaches equilibria by having undergone only physical and little chemical change. In this state, the biomass is less reactive, and the formation of an activated complex takes a prolonged time [49,50]. High ΔS values, however, occur during complex reactivity and rapid activation [34].

4. Conclusion

The *Canarium schweinfurthii* hard-shell had chemical structures with functional groups identical to those found in established biomass sources and contain 99 wt% carbon, 1.73 MJ/kg calorific value and 74.31% volatile matter.

The hard-shell loses around 56.45 wt% of its weight during the active pyrolysis stage, with E_α values of 46–221 kJ/mol, 36–223 kJ/mol, and 30–213 kJ/mol according FWO, KAS, and Starink methods respectively. The contraction and diffusion mechanisms mostly propagated the complex, multi-step reactions of the overall hard-shell pyrolysis.

The activation energies, Gibbs free energies and enthalpy values for hard-shell pyrolysis reactions are 103–233 kJ/mol, 169–170 kJ/mol, and 30–124 kJ/mol, respectively. Then, the pyrolysis required energy to progress to completion, and that the reactions were irreversible, highly random, and non-spontaneous.

The hard-shell was degraded via intermediate pyrolysis under the best conditions of 550 °C and a heating rate of 20 °C/min for 30 min to produce a maximum amount of liquid with 24 wt% bio-oil.

The bio-oils from hard-shell pyrolysis are saturated with oxygenated compounds, according to the FTIR and GC-MS results. They are, however, suitable for use as liquid biofuels precursors due to their less acidity and adequate calorific values ranging from 26.32 to 27.83 MJ/kg.

The biochar of the hard-shell had a high carbon content and calorific values ranging from 25.45 to 28.61 MJ/kg and low sulphur and nitrogen contents, indicating its eligibility as a renewable solid fuel for heating.

Author contribution statement

Kabir Garba: Conceived and designed the experiments; Performed the experiments; Analyzed and interpreted the data; Contributed reagents, materials, analysis tools or data; Wrote the paper.

Isah Yakub Mohammed; Yousif Abdalla Abakr: Analyzed and interpreted the data.

Yusuf Makarfi Isa; Bassim H. Hameed: Analyzed and interpreted the data; Contributed reagents, materials, analysis tools or data.

Lawan Garba Abubakar: Analyzed and interpreted the data; Wrote the paper.

Funding statement

This work was supported by Tertiary Education Trust Fund of Nigeria [TETFund/DR & D/CE/NRF/2019/STI/49].

Data availability statement

Data will be made available on request.

Declaration of interest's statement

The authors declare no conflict of interest.

References

[1] G. Kabir, B.H. Hameed, Recent progress on catalytic pyrolysis of lignocellulosic biomass to high- grade bio-oil and bio-chemicals, Renew. Sustain. Energy Rev. 70 (2016) 945–967, https://doi.org/10.1016/j.rser.2016.12.001.

[2] D. Wang, P. Jiang, H. Zhang, W. Yuan, Biochar production and applications in agro and forestry systems : a review, Sci. Total Environ. 723 (2020), 137775, https://doi.org/10.1016/j.scitotenv.2020.137775.

[3] S. Meyer, B. Glaser, P. Quicker, Technical , economical , and climate-related aspects of biochar production technologies : a literature review, Environ. Sci. Technol. (2011) 9473–9483.

[4] P.A. Costa, M.A. Barreiros, A.I. Mouquinho, P. Oliveira, F. Paradela, F.A. Costa, Slow pyrolysis of cork granules under nitrogen atmosphere : by-products characterization and their potential valorization, Biofuel Res. J. 33 (2022) 1562–1572, https://doi.org/10.18331/BRJ2022.9.1.3.

[5] H. Iyodo, K. Garba, S. Isa, L. Garba, Recent advances on strategies for upgrading biomass pyrolysis vapour to value-added bio-oils for bioenergy and chemicals, Sustain. Energy Technol. Assessments 55 (2023), 102984, https://doi.org/10.1016/j.seta.2022.102984.

[6] T. Kan, V. Strezov, T.J. Evans, Lignocellulosic biomass pyrolysis : a review of product properties and effects of pyrolysis parameters, Renew. Sustain. Energy Rev. 57 (2016) 1126–1140, https://doi.org/10.1016/j.rser.2015.12.185.

[7] G. Kabir, I.Y. Mohammed, Y.A. Abakr, H.H. Bassim, Intermediate pyrolysis of desert date shell for conversion to high-quality biomaterial resources, Chem. Eng. Technol. 45 (2022) 1213–1227, https://doi.org/10.1002/ceat.202200095.

[8] Y. Makkawi, Y. El Sayed, M. Salih, P. Nancarrow, S. Banks, T. Bridgwater, Fast pyrolysis of date palm (Phoenix dactylifera) waste in a bubbling fluidized bed reactor, Renew. Energy 143 (2019) 719–730, https://doi.org/10.1016/j.renene.2019.05.028.

[9] R.E. Guedes, A.S. Luna, A.R. Torres, Operating parameters for bio-oil production in biomass pyrolysis: a review, J. Anal. Appl. Pyrolysis 129 (2018) 134–149, https://doi.org/10.1016/j.jaap.2017.11.019.

[10] P. Sakulkit, A. Palamanit, R. Dejchanchaiwong, P. Reubroycharoen, Characteristics of pyrolysis products from pyrolysis and co-pyrolysis of rubber wood and oil palm trunk biomass for biofuel and value-added applications, J. Environ. Chem. Eng. 8 (2020), 104561, https://doi.org/10.1016/j.jece.2020.104561.

[11] G. Kabir, A.T.M. Din, B.H. Hameed, Pyrolysis of oil palm mesocarp fiber and palm frond in a slow-heating fixed- bed reactor: a comparative study, Bioresour. Technol. 241 (2017) 563–572, https://doi.org/10.1016/j.biortech.2017.05.180.

[12] J. V Karaeva, S.S. Timofeeva, S.I. Islamova, A. V Gerasimov, Pyrolysis kinetics of new bioenergy feedstock from anaerobic digestate of agro-waste by thermogravimetric analysis, J. Environ. Chem. Eng. 10 (2022), 107850, https://doi.org/10.1016/j.jece.2022.107850.

[13] R. Keey, W. Lun, M. Yee, X. Yee, M. Huan, P. Nai, Y. Yek, N. Ling, C. Kui, C. Tung, S. Shiung, Oil palm waste : an abundant and promising feedstock for microwave pyrolysis conversion into good quality biochar with potential multi-applications, Process Saf. Environ. Protect. 115 (2018) 57–69, https://doi.org/10.1016/j.psep.2017.10.005.

[14] J. He, V. Strezov, T. Kan, H. Weldekidan, S. Asumadu-Sarkodie, R. Kumar, Effect of temperature on heavy metal(loid) deportment during pyrolysis of Avicennia marina biomass obtained from phytoremediation, Bioresour. Technol. 278 (2019) 214–222, https://doi.org/10.1016/j.biortech.2019.01.101.
[15] W.A. Khanday, G. Kabir, B.H. Hameed, Catalytic pyrolysis of oil palm mesocarp fibre on a zeolite derived from low-cost oil palm ash, Energy Convers. Manag. 127 (2016) 265–272, https://doi.org/10.1016/j.enconman.2016.08.093.
[16] N.M.T. Al-Layla, L.A. Saleh, A.B. Fadhil, Liquid bio-fuels and carbon adsorbents production via pyrolysis of non-edible feedstock, J. Anal. Appl. Pyrolysis 156 (2021), 105088, https://doi.org/10.1016/j.jaap.2021.105088.
[17] P. Cross, C. Mukarakate, M. Nimlos, D. Carpenter, B.S. Donohoe, J.A. Mayer, J.C. Cushman, B. Neupane, G.C. Miller, S. Adhikari, Fast pyrolysis of opuntia ficus-indica (prickly pear) and grindelia squarrosa (gumweed), Energy Fuel. 32 (2018) 3510–3518, https://doi.org/10.1021/acs.energyfuels.7b03752.
[18] S. Shiung, R. Keey, A. Jusoh, C. Tung, F. Nasir, H.A. Chase, Progress in waste oil to sustainable energy , with emphasis on pyrolysis techniques, Renew. Sustain. Energy Rev. 53 (2016) 741–753, https://doi.org/10.1016/j.rser.2015.09.005.
[19] A.C.M. Loy, D.K.W. Gan, S. Yusup, B.L.F. Chin, M.K. Lam, M. Shahbaz, P. Unrean, M.N. Acda, E. Rianawati, Thermogravimetric kinetic modelling of in-situ catalytic pyrolytic conversion of rice husk to bioenergy using rice hull ash catalyst, Bioresour. Technol. 261 (2018) 213–222, https://doi.org/10.1016/j.biortech.2018.04.020.
[20] P. Das, D. Mondal, S. Maiti, Thermochemical conversion pathways of Kappaphycus alvarezii granules through study of kinetic models, Bioresour. Technol. 234 (2017) 233–242, https://doi.org/10.1016/j.biortech.2017.03.007.
[21] A. Al-rumaihi, P. Parthasarathy, A. Fernandez, T. Al-ansari, G. Mckay, Thermal degradation characteristics and kinetic study of camel manure pyrolysis, J. Environ. Chem. Eng. 9 (2021), 106071, https://doi.org/10.1016/j.jece.2021.106071.
[22] N. Gao, A.T. Sipra, C. Quan, Thermogravimetric analysis and pyrolysis product characterization of municipal solid waste using sludge fly ash as additive, Fuel 281 (2020), 118572, https://doi.org/10.1016/j.fuel.2020.118572.
[23] A. Kumar, R.K. Mishra, Pyrolysis of low-value waste miscanthus grass_ Physicochemical characterization, pyrolysis kinetics, and characterization of pyrolytic end products, Process Saf. Environ. Protect. 163 (2022) 68–81, https://doi.org/10.1016/j.psep.2022.05.022.
[24] S. Fang, Z. Yu, Y. Lin, S. Hu, Y. Liao, X. Ma, Thermogravimetric analysis of the co-pyrolysis of paper sludge and municipal solid waste, Energy Convers. Manag. 101 (2015) 626–631, https://doi.org/10.1016/j.enconman.2015.06.026.
[25] J. Chen, X. Fan, B. Jiang, L. Mu, P. Yao, H. Yin, X. Song, Pyrolysis of oil-plant wastes in a TGA and a fixed-bed reactor : thermochemical behaviors , kinetics , and products characterization, Bioresour. Technol. 192 (2015) 592–602, https://doi.org/10.1016/j.biortech.2015.05.108.
[26] M.S. Ahmad, M.A. Mehmood, S.T.H. Taqvi, A. Elkamel, C.G. Liu, J. Xu, S.A. Rahimuddin, M. Gull, Pyrolysis, kinetics analysis, thermodynamics parameters and reaction mechanism of Typha latifolia to evaluate its bioenergy potential, Bioresour. Technol. 245 (2017) 491–501, https://doi.org/10.1016/j.biortech.2017.08.162.
[27] C.T. Chong, G.R. Mong, J.H. Ng, W.W.F. Chong, F.N. Ani, S.S. Lam, H.C. Ong, Pyrolysis characteristics and kinetic studies of horse manure using thermogravimetric analysis, Energy Convers. Manag. 180 (2019) 1260–1267, https://doi.org/10.1016/j.enconman.2018.11.071.
[28] A. Nasrullah, A.S. Khan, S.Z. Khan, A. Inayat, T.M. Fagieh, E.M. Bakhsh, K. Akhtar, S.B. Khan, I.U. Din, Kinetics and thermodynamic study of Calligonum polygonoides pyrolysis using model-free methods, Process Saf. Environ. Protect. 160 (2022) 130–138, https://doi.org/10.1016/j.psep.2022.01.084.
[29] L.D.M.S. Borel, T.S. Lira, J.A. Ribeiro, C.H. Ataide, M.A.S. Barrozo, Pyrolysis of brewer's spent grain: kinetic study and products identification, Ind. Crop. Prod. 121 (2018) 388–395, https://doi.org/10.1016/j.indcrop.2018.05.051.
[30] R.N. Mandapati, P.K. Ghodke, Kinetics of pyrolysis of cotton stalk using model-fitting and model-free methods, Fuel 303 (2021), 121285, https://doi.org/10.1016/j.fuel.2021.121285.
[31] H.I. Mohammed, K. Garba, S.I. Ahmed, L.G. Abubakar, Thermodynamics and kinetics of Doum (Hyphaene thebaica) shell using thermogravimetric analysis: a study on pyrolysis pathway to produce bioenergy, Renew. Energy 200 (2022) 1275–1285, https://doi.org/10.2139/ssrn.4152713.
[32] D. Mallick, M.K. Poddar, P. Mahanta, V.S. Moholkar, Discernment of synergism in pyrolysis of biomass blends using thermogravimetric analysis, Bioresour. Technol. 261 (2018) 294–305, https://doi.org/10.1016/j.biortech.2018.04.011.
[33] S. Ceylan, Thermokinetic analysis and product characterization of waste tire-hazelnut shell co-pyrolysis : TG-FTIR and fixed bed reactor study, J. Environ. Chem. Eng. 9 (2021), 106165, https://doi.org/10.1016/j.jece.2021.106165.
[34] J. Ma, H. Luo, Y. Li, Z. Liu, D. Li, C. Gai, W. Jiao, Pyrolysis kinetics and thermodynamic parameters of the hydrochars derived from co-hydrothermal carbonization of sawdust and sewage sludge using thermogravimetric analysis, Bioresour. Technol. 282 (2019) 133–141, https://doi.org/10.1016/j.biortech.2019.03.007.
[35] D. Lopez-Gonzalez, M. Fernandez-Lopez, J.L. Valverde, L. Sanchez-Silva, Gasification of lignocellulosic biomass char obtained from pyrolysis: kinetic and evolved gas analyses, Energy 71 (2014) 456–467, https://doi.org/10.1016/j.energy.2014.04.105.
[36] S. Vyazovkin, A.K. Burnham, J.M. Criado, L.a. Perez-Maqueda, C. Popescu, N. Sbirrazzuoli, ICTAC Kinetics Committee recommendations for performing kinetic computations on thermal analysis data, Thermochim. Acta 520 (2011) 1–19, https://doi.org/10.1016/j.tca.2011.03.034.
[37] J.E. White, W.J. Catallo, B.L. Legendre, Biomass pyrolysis kinetics: a comparative critical review with relevant agricultural residue case studies, J. Anal. Appl. Pyrolysis 91 (2011) 1–33, https://doi.org/10.1016/j.jaap.2011.01.004.
[38] H. Li, S. Niu, C. Lu, Thermal characteristics and kinetic calculation of Castor oil pyrolysis, Procedia Eng. 205 (2017) 3711–3716, https://doi.org/10.1016/j.proeng.2017.10.297.
[39] I.Y. Mohammed, G. Kabir, Y.A. Abakr, M. Atogiba, A. Apasiku, F.K. Kazi, L.G. Abubakar, Bioenergy potential of millet chaff via thermogravimetric analysis and combustion process simulation using aspen plus, Clean. Chem. Eng. 3 (2022), 100046, https://doi.org/10.1016/j.clce.2022.100046.
[40] R.K. Mishra, K. Mohanty, Pyrolysis kinetics and thermal behavior of waste sawdust biomass using thermogravimetric analysis, Bioresour. Technol. 251 (2018) 63–74, https://doi.org/10.1016/j.biortech.2017.12.029.
[41] Y. Lin, X. Ma, Z. Yu, Y. Cao, Investigation on thermochemical behavior of co-pyrolysis between oil-palm solid wastes and paper sludge, Bioresour. Technol. 166 (2014) 444–450, https://doi.org/10.1016/j.biortech.2014.05.101.
[42] S.R. Naqvi, Y. Uemura, S.B. Yusup, Catalytic pyrolysis of paddy husk in a drop type pyrolyzer for bio-oil production: the role of temperature and catalyst, J. Anal. Appl. Pyrolysis 106 (2014) 57–62, https://doi.org/10.1016/j.jaap.2013.12.009.
[43] R. Saikia, B. Baruah, D. Kalita, K.K. Pant, N. Gogoi, R. Kataki, CharacterizationPyrolysis and kinetic analyses of a perennial grass (saccharum ravannae L.) from north-east India: optimization through response surface, Bioresour. Technol. (2018), https://doi.org/10.1016/j.biortech.2018.01.054.
[44] V. Dhyani, T. Bhaskar, A comprehensive review on the pyrolysis of lignocellulosic biomass, Renew. Energy 129 (2018) 695–716, https://doi.org/10.1016/j.renene.2017.04.035.
[45] C. Setter, F.T.M. Silva, M.R. Assis, C.H. Ataide, P.F. Trugilho, T.J.P. Oliveira, Slow pyrolysis of coffee husk briquettes: characterization of the solid and liquid fractions, Fuel (2020) 261, https://doi.org/10.1016/j.fuel.2019.116420.
[46] S.A. Akinyemi, B.B. Nyakuma, A. Jauro, O.F. Adebayo, O.A. OlaOlorun, A.K. Adegoke, A.O. Aturamu, A. Adetunji, W.M. Gitari, R. Mudzielwana, Mineralogy, physicochemical and oxidative thermal analyses of Cretaceous coals from the Benue Trough, Nigeria, Energy Geosci 2 (2021) 129–135, https://doi.org/10.1016/j.engeos.2020.07.001.
[47] D. Pradhan, R.K. Singh, H. Bendu, R. Mund, Pyrolysis of Mahua seed (Madhuca indica) - production of biofuel and its characterization, Energy Convers. Manag. 108 (2016) 529–538, https://doi.org/10.1016/j.enconman.2015.11.042.
[48] O. Çepelioğullar, H. Haykiri-Acma, S. Yaman, Kinetic modelling of RDF pyrolysis: model-fitting and model-free approaches, Waste Manag. 48 (2016) 275–284, https://doi.org/10.1016/j.wasman.2015.11.027.
[49] R. Kaur, P. Gera, M.K. Jha, T. Bhaskar, Pyrolysis kinetics and thermodynamic parameters of castor (Ricinus communis) residue using thermogravimetric analysis, Bioresour. Technol. 250 (2018) 422–428, https://doi.org/10.1016/j.biortech.2017.11.077.
[50] A.H. Rony, L. Kong, W. Lu, M. Dejam, H. Adidharma, K.A.M. Gasem, Y. Zheng, U. Norton, M. Fan, Kinetics, thermodynamics, and physical characterization of corn stover (Zea mays) for solar biomass pyrolysis potential analysis, Bioresour. Technol. 284 (2019) 466–473, https://doi.org/10.1016/j.biortech.2019.03.049.